JACS
JOURNAL OF THE AMERICAN CHEMICAL SOCIETY
Article
Cite This: J. Am. Chem. Soc. 2018, 140, 7519−7525
pubs.acs.org/JACS

Presence of Short Intermolecular Contacts Screens for Kinetic Stability in Packing Polymorphs

Geoffrey E. Purdum,[†] Nicholas G. Telesz,[‡] Karol Jarolimek,[‡] Sean M. Ryno,[‡] Thomas Gessner,[§] Nicholas C. Davy,[†] Anthony J. Petty, II,[‡] Yonggang Zhen,[∥] Ying Shu,[⊥] Antonio Facchetti,[#] Gavin E. Collis,[⊥] Wenping Hu,[∥,^] Chao Wu,[§] John E. Anthony,[‡] R. Thomas Weitz,[§,○] Chad Risko,[‡] and Yueh-Lin Loo*[,†,▽]

[†]Department of Chemical and Biological Engineering, Princeton University, Princeton, New Jersey 08544, United States
[‡]Department of Chemistry, University of Kentucky, Lexington, Kentucky 40506, United States
[§]BASF SE, 67056 Ludwigshafen, Germany
[∥]Institute of Chemistry, Chinese Academy of Sciences, Beijing 100190, China
[⊥]Commonwealth Scientific and Industrial Research Organisation, Clayton South Victoria 3169, Australia
[#]Flexterra Corporation, Skokie, Illinois 60077, United States
[▽]Andlinger Center for Energy and the Environment, Princeton University, Princeton, New Jersey 08544, United States

Supporting Information

ABSTRACT: Polymorphism is pervasive in molecular solids. While computational predictions of the molecular polymorphic landscape have improved significantly, identifying which polymorphs are preferentially accessed and experimentally stable remains a challenge. We report a framework that correlates short intermolecular contacts with polymorphic stability. The presence of short contacts between neighboring molecules prevents structural rearrangement and stabilizes the packing arrangement, even when the stabilized polymorph is not enthalpically favored. In the absence of such intermolecular short contacts, the molecules have added degrees of freedom for structural rearrangement, and solid−solid polymorphic transformations occur readily. Starting with a series of core-halogenated naphthalene tetracarboxylic diimides, we establish this framework with the packing polymorphs of more than 20 compounds, ranging from molecular semiconductors to pharmaceutics and biological building blocks. This framework, widely applicable across molecular solids, can help refine computational predictions by identifying the polymorphs that are kinetically stable.

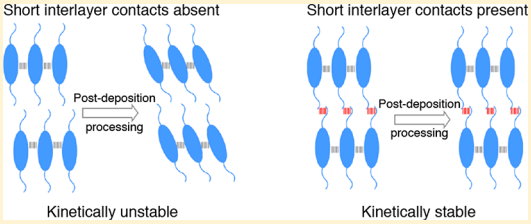

INTRODUCTION

The solid-state packing arrangement of organic molecules critically impacts their materials properties, from those as general as solubility and thermal stability to ones as specific as bioavailability and charge transport. A consequence of the noncovalent interactions[1] uniquely at play in molecular materials is that more than one in two molecules displays polymorphism, or the ability to adopt multiple packing motifs.[2] The ability to predict the packing polymorphs of new materials a priori, and access them accordingly, can thus impact industries as wide ranging as pharmaceutics,[3,4] food,[5] and explosives[6] and disciplines as disparate as biology,[7] agriculture,[8] and organic electronics.[9,10] While computational efforts have progressed substantially in predicting the most thermodynamically stable packing arrangements, there often exists many plausible solid-state structures with free energy differences that are less than 1 kcal/mol.[2,11−13] Comparable in magnitude to thermal fluctuations (k_BT) at room temperature, these different polymorphs are considered to be practically isoenergetic. Yet, for many molecules that exhibit polymorphism, specific packing polymorphs are often preferentially accessed and these need not be the most thermodynamically stable packing arrangement. One such case is 5-methyl-2-[(2-nitrophenyl)amino]-3-thiophenecarbonitrile, more commonly known as ROY. While its form Y crystal structure is the most thermodynamically stable phase, ROY, of the same conformer, can crystallize into two other structurally resolved and distinct packing arrangements and of the other conformer another four distinct packing polymorphs that are each stable at ambient conditions for months to years.[14] As another example, the β phase of anhydrous guanine is uniquely observed under physiological conditions despite predictions that its α phase is thermodynamically favored.[15,16] Adding to these examples are empirical studies on pharmaceutics in which fluorination is used to enhance bioavailability, though the exact influence fluorine has on the relative stabilities of different polymorphs is still not well understood.[17,18] Collectively, these results indicate that

Received: February 5, 2018
Published: May 25, 2018

DOI: 10.1021/jacs.8b01421
J. Am. Chem. Soc. 2018, 140, 7519−7525

calculations to determine the most thermodynamically stable polymorph alone do not provide sufficient insight into which polymorph will be kinetically stable with extended lifetimes at ambient conditions. Herein, we describe a framework, generalizable across a wide range of molecular materials, that directly correlates intermolecular contacts with kinetic stability of packing polymorphs. Polymorphs that exhibit short contacts between neighboring molecules are effectively arrested and their solid−solid phase transformations to other packing arrangements precluded, even when the latter ones are enthalpically favored.

RESULTS AND DISCUSSION

We investigated the polymorphic stability of a series of naphthalene tetracarboxylic diimide (NTCDI) derivatives, whose chemical structures are shown in Figure 1a. NTCDI

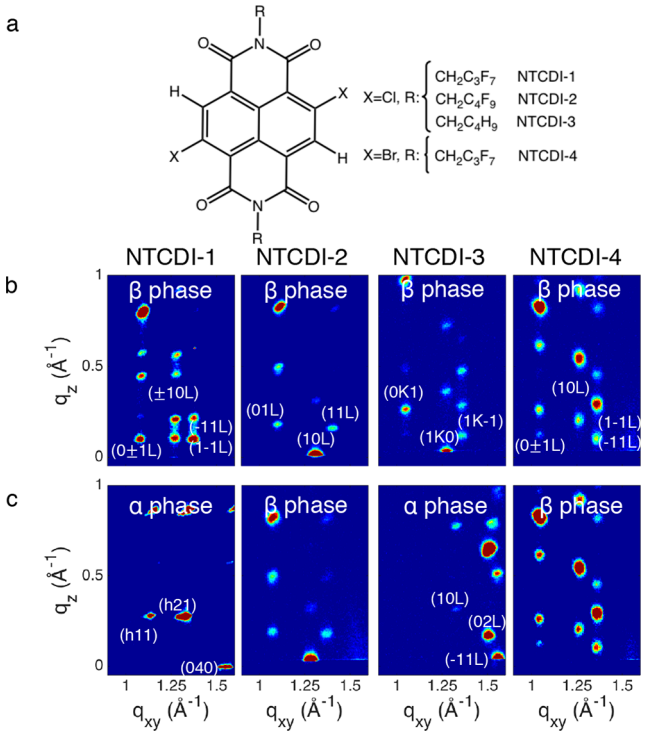

Figure 1. (a) Chemical structures of NTCDI derivatives examined in this study. (b and c) GIXD patterns of as-evaporated and solvent-vapor annealed NTCDI thin films, respectively.

derivatives crystallize into one of two polymorphs when grown at quasi-equilibrium conditions: single crystals of their α phase are accessed via solution recrystallization and single crystals of their β phase are accessed through physical-vapor transport (Table S1).[19,20] Single-crystal X-ray crystallography confirms that small changes to the molecular chemistry (e.g., the substitution of hydrogenated alkyl chains with perfluorinated ones, the extension of perfluorinated alkyl chains by one fluoromethylene unit, and the replacement of Cl with Br on the conjugated core) do not dramatically alter the adopted crystal structures. In a similar fashion, periodic DFT calculations indicate that the subtle changes in substituent chemistries do not significantly alter the cohesive energies of the crystal structures (Table S2). In fact, the cohesive energy difference between the α and β polymorphs of each NTCDI derivative is small, ranging in magnitude from 0.5 to 1.2 kcal/mol.

Figure 1b,c shows grazing-incidence X-ray diffraction (GIXD) patterns of as-evaporated and solvent-vapor annealed thin films of the NTCDI derivatives, respectively. The GIXD patterns of the as-evaporated thin films are consistent with those of the β phases of each derivative. Two-body symmetry-adapted perturbation theory (SAPT) calculations reveal a modest preference for face-to-face configurations found in the β phases compared to those of the α phases (Tables S3−S14), which may help explain why the β phases are consistently accessed on deposition. On post-deposition solvent-vapor annealing, the GIXD patterns of NTCDI-2 and -4 remain invariant, whereas those of NTCDI-1 and -3 change drastically, matching those of their α-phase polymorphs instead. This observation implicates a divergence in polymorphic stability despite nominal differences in the packing arrangements of the β phases of the NTCDI derivatives. In addition to solvent-vapor annealing, thermally annealing β-phase films also converts NTCDI-3 to its α phase, presenting an opportunity to quantify its transformation kinetics. In situ GIXD during isothermal annealing, shown in Figure S1, indicates that this β-to-α transformation follows second-order Avrami kinetics with an energy barrier of 25 ± 2 kcal/mol. These results indicate a nucleation and growth mechanism, consistent with our previous report on NTCDI-1.[10] Given that this transformation happens via both thermal and solvent-vapor annealing in NTCDI-3, via only solvent-vapor annealing in NTCDI-1, and not at all in NTCDI-2 and -4, we surmise the energy barrier for this β-to-α polymorphic transformation to be the greatest in NTCDI-2 and -4. We further speculate that this barrier is responsible for stabilizing their β phases.

Although the molecular arrangements in the β phase of each derivative are qualitatively similar, the modest differences in chemical structures manifest themselves through distinctive noncovalent intermolecular interactions. As a proxy for the strength and nature of a subset of the full noncovalent intermolecular interactions in the solid state, we define an intermolecular contact (hereafter simply referred to as contact) as the distance between any two atoms on neighboring molecules. We classify these contacts as short when this distance is less than the sum of the Bondi[21] van der Waals (vdW) radii of the corresponding atoms. With this quantification framework in mind, we turn to Figure 2, which highlights the discrete molecular layers within the solid-state structures of the NTCDI derivatives. While these derivatives exhibit similar intralayer short contacts in their β phases, the

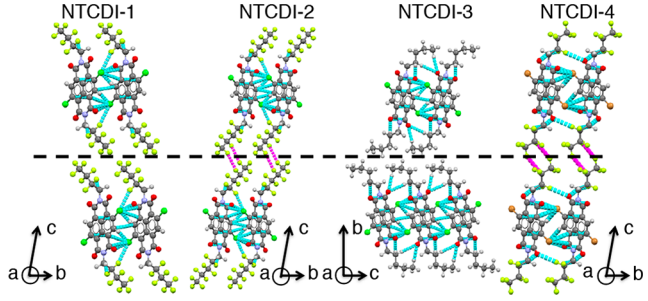

Figure 2. Crystal structures of β phase NTCDI derivatives viewed along their a-axes. The cyan lines depict intralayer short contacts, and magenta lines depict interlayer short contacts, which are present between layers of NTCDI-2 and -4 but not between layers of NTCDI-1 or -3. The dashed black line is a guide to the eye to distinguish between molecular layers.

DOI: 10.1021/jacs.8b01421
J. Am. Chem. Soc. 2018, 140, 7519−7525

interlayer contacts are qualitatively different. Specifically, Figure 2 reveals the presence of short interlayer contacts in the β phases of NTCDI-2 and -4 that are not present in the β phases of NTCDI-1 and -3. This difference in interlayer contacts among the NTCDI derivatives is further confirmed by Hirshfeld analyses[22] (Figure S2). Table 1 summarizes the interlayer contacts of the NTCDI derivatives in this series. Interestingly, the presence of short interlayer contacts in the β phases of NTCDI-2 and -4 correlates with their enhanced stability, and, by the same token, the absence of such contacts in the β phases of NTCDI-1 and -3 positively correlates with their ability to undergo solid−solid polymorphic transformations.

Table 1. Intermolecular Contact Distances[a]

compound/polymorph	CCDC no.	shortest interlayer contact − ΣvdW radii/type of contact	stable to post-deposition processing?
NTCDI-1/β phase	1018034	+0.144/F···F	N
NTCDI-2/β phase	1570695	−0.029/F···F	Y
NTCDI-3/β phase	1570697	+0.162/C···H	N
NTCDI-4/β phase	1570982	−0.033/F···F	Y
TIPS Pn/β phase	172476	+0.145/C···H	N
TIPS Pn/form IIb	1570911	+0.108/C···H	N
C6 DBTDT/β phase	NA[b]	+0.127/C···H	N
TMS DBC/α phase	890408	−0.003/C···H	Y
TES Pn/α phase	1028702	−0.049/C···H	Y
offset TIPS Pn/form I	172477	−0.016/C···H	Y
PDIF-CN2/β phase	247207	−0.240/F···F	Y

[a]All units are in Å. [b]The β-phase structure of C6 DBTDT was calculated and reported in ref 25.

Short contacts between atoms on the periphery of aromatic hydrocarbons, such as these interlayer contacts, are energetically destabilizing compared to equilibrium contact distances. While attractive forces (e.g., dispersion, permanent electrostatics, induction, and charge penetration) are often credited with holding together molecular solids, the combination of repulsive forces arising from exchange and charge penetration effects that turn on at short distances can stabilize packing motifs by opposing shifts from the equilibrium molecular arrangement.[23,24] Noting also that the short contacts that are present in the NTCDI derivatives are inherently many bodied in nature, we surmise that the interlayer short contacts in NTCDI-2 and -4 stabilize the β phase, impeding any transformation to its α phase. Similarly, the lack of interlayer short contacts in NTCDI-1 and -3 provides an added degree of freedom that facilitates molecular rearrangement on post-deposition processing to transform into their respective α phases.

We note, however, that this simple, short contact framework is limited by the accuracy of the resolved crystal structures. The atomic, and thus molecular, coordinates of a resolved crystal structure are spatiotemporally averaged over fluctuations about their equilibrium positions. Because most single-crystal diffraction measurements occur at low temperatures (ca. 100 K) in which thermal fluctuations are dampened, molecules can be effectively "frozen" into positions that are closer together than their equilibrium structures at ambient conditions. Indeed, increasing temperature typically results in the expansion of the unit cell. To assess how much intermolecular contacts can vary as a function of temperature, we consider orthorhombic rubrene, whose crystal structure has been determined at multiple temperatures spanning 100−293 K.[26] Orthorhombic rubrene exhibits short interlayer C···H contacts between molecular layers along its *a*-axis. While the *a*-axis expands by 0.15 Å with temperature from 100 to 293 K, the C···H interlayer contact only expands by 0.04 Å, highlighting that intermolecular contacts are substantially less sensitive to temperature than the unit cell dimensions themselves. Further, previous studies suggest that contacts involving halogens can increase by 0.03−0.08 Å between 100 and 300 K.[27] Despite the uncertainties such temperature dependence introduce to short contact determination, our analysis provides upper bounds on the estimated short contacts when crystal structures that are resolved at low temperatures are used. That is to say, if the crystal structure of a compound does not exhibit short contacts at low temperatures, it is highly unlikely it will do so at ambient conditions. Further, our framework relies on comparing the contact distance to the vdW radii determined by Bondi. Despite his disclaimer that these values "may not be suitable for the calculation of contact distances in crystals",[21] data mining of thousands of crystal structures deposited in the Cambridge Structural Database (CSD) have, on the contrary, shown contact distances with discrepancies that are less than 0.05 Å with Bondi's vdW radii.[28] Finally, the experimentally determined average distance of many intermolecular nonbonded contacts, especially those involving carbon, have been shown to be greater than the sum of their vdW radii,[28] suggesting that short-contact analysis using Bondi vdW radii provides a lower bound. While we recognize the shortcomings of our simplistic analysis, we believe it still quantitatively captures the short contacts in molecular crystals because the errors introduced by relying on crystal structures that are resolved at low temperatures to first order cancel out those introduced by the Bondi framework, given that the former overestimates and the latter underestimates the contact distances by comparable magnitudes.

With these limitations in mind, we assessed the generality of this framework by evaluating the polymorphic stability of additional molecules that have either been experimentally shown or computationally predicted to be polymorphic. 6,13-bis(triisopropylsilylethynyl)pentacene (TIPS Pn) and dihexyl-substituted dibenzo[*d*,*d*′]thieno[3,2-*b*;4,5-*b*′]dithiophene (C6 DBTDT) were chosen as negative control experiments due to the absence of short interlayer contacts in their known crystal structures.[25,29−31] We thus expect the polymorphs of each to be unstable to post-deposition annealing, resulting in solid−solid phase transformations. Conversely, 6,13-bis(triethylsilylethynyl)pentacene (TES Pn) and 7,14-bis(trimethylsilylethynyl)dibenzo[*b*,*def*]-chrysene (TMS DBC) were investigated as positive control experiments. The presence of short interlayer contacts in the α-phase crystal structures of each should stabilize these phases, restricting any polymorphic transformations.[32,33] The crystal structures of each molecule are shown in Figure S3.

TIPS Pn has two resolved bulk crystal structures, the β phase and form IIb, and numerous other experimentally observed thin-film polymorphs. Interlayer short contacts are notably absent in both known crystal structures. Given this absence, coupled with the predicted energetic difference of less than 2 kcal/mol between both polymorphs,[34] we expect TIPS Pn to undergo polymorphic transformations upon post-deposition annealing. Starting with spun-cast amorphous films of TIPS Pn, we imposed post-deposition processing in the form of solvent-

DOI: 10.1021/jacs.8b01421
J. Am. Chem. Soc. 2018, 140, 7519−7525

vapor and/or thermal annealing to induce crystallization, consistent with previous studies.[35,36] GIXD patterns corresponding to these films are shown in Figure 3a,b. Comparison

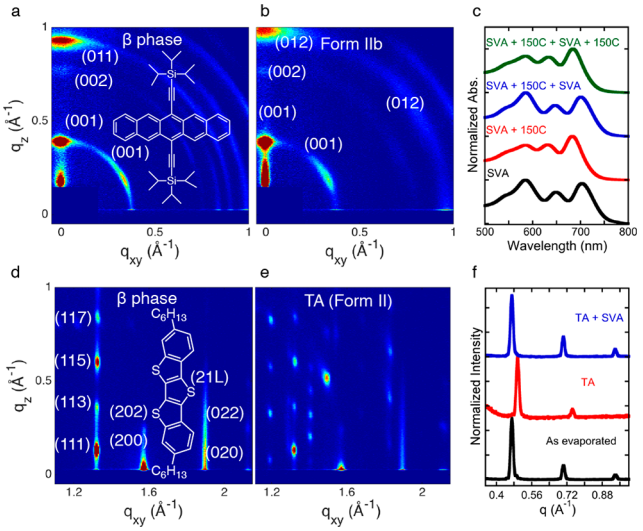

Figure 3. (a and b) GIXD patterns of solvent-vapor and thermally annealed TIPS Pn thin films adopting its β phase and form IIb, respectively. The chemical structure of TIPS Pn is shown in the inset. (c) Absorbance spectra of TIPS Pn after sequential post-deposition thermal and solvent-vapor annealing, demonstrating reversible access to both polymorphs. (d and e) GIXD pattern of as-evaporated and thermally annealed C6 DBTDT thin films adopting its β phase and form II, respectively. The chemical structure of C6 DBTDT is shown in the inset. (f) Out-of-plane X-ray diffraction traces of an evaporated film after sequential post-deposition thermal annealing at 180 °C and solvent-vapor annealing with acetone, showing the reversible access of its β phase with solvent-vapor annealing.

of the GIXD patterns indicates that solvent-vapor annealing converts the amorphous film to its β phase, whereas thermally annealing the amorphous film above 125 °C results in a crystalline phase consistent with the previously reported form IIb. We then subjected the solvent-vapor annealed films to thermal annealing and vice versa. As evidenced by the UV−vis absorbance in Figure 3c, thermal annealing results in a polymorphic transformation out of the β phase and into form IIb, and solvent-vapor annealing reverses the transformation from form IIb to the β phase. This transformation occurs very rapidly, consistent with a recent report of its Martensitic nature.[30] The ability to transform out of both the β phase and form IIb of TIPS Pn is consistent with the lack of interlayer short contacts in the crystal structures of both polymorphs, the presence of which would otherwise stabilize their intermolecular packing arrangements and inhibit structural rearrangement.

Similar to TIPS Pn, C6 DBTDT has been shown to adopt multiple polymorphs, but only one of these, the α phase, has been structurally resolved via single-crystal X-ray crystallography. A combination of selected-area electron diffraction and DFT calculations indicates the β phase to adopt a layered herringbone structure with noninteracting layers.[25] Given our framework, the absence of short interlayer contacts in both polymorphs suggests neither should be stable to post-deposition annealing. To investigate, thin films of C6 DBTDT were deposited via thermal evaporation and subjected to sequential post-deposition processing of thermal and solvent-vapor annealing. GIXD patterns of these films, shown in Figure 3d,e, indicate that as-evaporated films adopt a crystal structure that is consistent with the β phase of C6 DBTDT, while thermal annealing transforms C6 DBTDT out of its β phase into a new, as-yet unreported polymorph (herein referred to as form II). Out-of-plane X-ray diffraction, shown in Figure 3f, and UV−vis absorbance, shown in Figure S4, reveal that polymorphic transformations between the β phase and form II of C6 DBTDT are fully reversible with sequential thermal and solvent-vapor annealing, consistent with our hypothesis, given that its β-phase crystal structure lacks interlayer short contacts. We further surmise that the form II crystal structure lacks short interlayer contacts given that we are able to reversibly transform out of this polymorph and into its β-phase polymorph.

TMS DBC has two structurally resolved polymorphs (α and β phase), both of which comprise discrete molecular layers. Short interlayer contacts are only present in the α phase, between the TMS substituent of a molecule and the DBC core of another molecule in the adjacent molecular layer. As such, we expect the α phase to be stable against solid−solid phase transformations on post-deposition annealing. TMS DBC was deposited via thermal evaporation; the GIXD patterns of an as-evaporated film, along with those after post-deposition processing, are shown in Figure 4a,c,e. Consistent with previous reports, as-evaporated thin films of TMS DBC adopt an unresolved structure, herein referred to as form I.[33] Thermally annealing does not induce any structural transformation in form I films, whereas toluene-vapor annealing induces a phase transformation to its α phase. Once in its α phase, however, none of the post-deposition processing routes we explored, including thermal annealing, solvent-vapor annealing, and combinations of the two, led to transformation out of this phase (Figure 4g). That we remain trapped in the α phase aligns with our hypothesis that short interlayer contacts preclude polymorphic transformations.

Of all of the molecules we sampled as control experiments, TES Pn is unique in that it has never experimentally exhibited polymorphism despite recent predictions that it could be polymorphic.[37] In its known α-phase structure, interlayer short contacts are present between the bulky TES group of one molecule and the pentacene core of another in the adjacent molecular layer. As with prior control experiments, we expected these short contacts to impede polymorphic transformations out of this phase. TES Pn films were deposited via spin-coating and subjected to post-deposition annealing; GIXD patterns of as-deposited, solvent-vapor annealed, and thermally annealed TES Pn films are shown in Figure 4b,d,f. As-deposited TES Pn films are highly crystalline, adopting an unresolved polymorph (herein form I). Subjecting films of form I to solvent-vapor and/or thermal annealing results in a polymorphic transformation to the known α phase. Additional solvent-vapor and/or thermal annealing does not induce transformation out of its α phase. Consistent with our framework, the presence of interlayer short contacts stabilizes the α phase and impedes any solid−solid phase transformations.

Both our positive and negative control experiments support the notion that short interlayer contacts arrest molecular packing. By the same token, these short contacts can limit accessibility to other polymorphs which can lead to different materials properties. Lattice matching and epitaxial growth are commonly used to access crystalline phases of inorganic semiconductors that are otherwise inaccessible; these approaches have recently been shown to impose control over

DOI: 10.1021/jacs.8b01421
J. Am. Chem. Soc. 2018, 140, 7519−7525

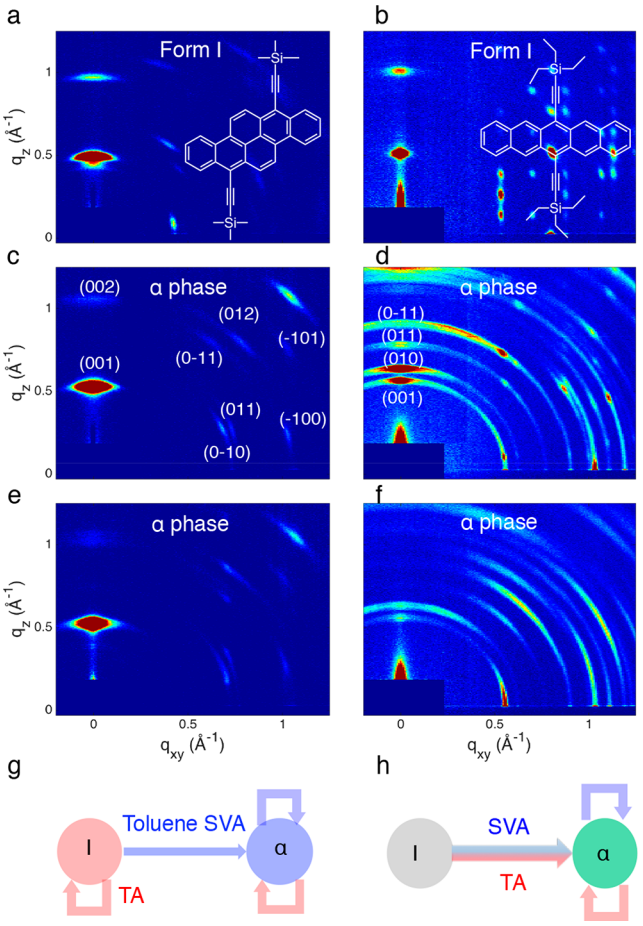

Figure 4. (a, c, and e) GIXD patterns of as-evaporated, toluene-vapor annealed, and sequential toluene-vapor and thermally annealed TMS DBC thin films. The chemical structure of TMS DBC is shown in the inset. As-evaporated films adopt form I while toluene-vapor annealing converts form I to its α phase. Subsequent annealing does not induce any structural changes, highlighting the irreversible polymorphic transformation between form I and its α phase. (b, d, and f) GIXD patterns of as-deposited, solvent-vapor annealed, and sequential solvent-vapor and thermally annealed TES Pn thin films. The chemical structure of TES Pn is shown in the inset. TES Pn adopts a new polymorph (form I) when deposited via spin-coating. Solvent-vapor and/or thermal annealing irreversibly convert form I to the α phase. (g and h) Schemes illustrating that TMS DBC and TES Pn, respectively, adopt their α phase irreversibly with solvent-vapor annealing.

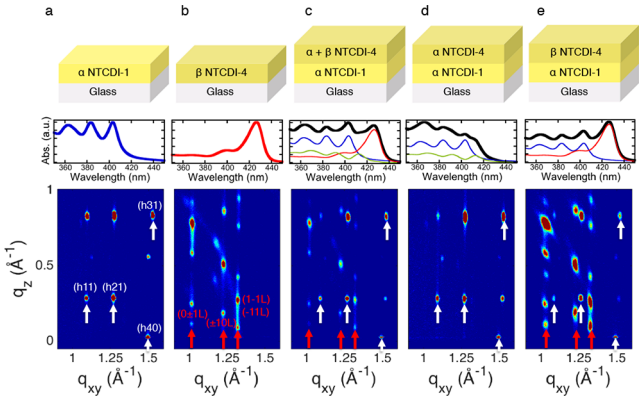

Figure 5. Schemes of thin film architecture (top row) with corresponding absorbance spectra (middle row) and GIXD patterns (bottom row). (a) α phase NTCDI-1 accessed through solvent-vapor annealing of a thermally evaporated thin film. (b) As-deposited NTCDI-4 adopts its β-phase. (c) A stack comprising as-evaporated NTCDI-4 atop the α-phase of NTCDI-1. (d) The stack shown in panel c after solvent-vapor annealing. (e) The stack shown in panel c after thermal annealing. The GIXD patterns in panels a and b have been indexed according to the crystal structures of the α and β polymorphs of NTCDI-1 and -4, respectively. White arrows highlight the reflections associated with the α phases of NTCDI-1 and -4; red arrows highlight the β phases of both compounds. The absorbance spectra of the stacked films are shown in black, while the contributions from α phase NTCDI-1, α phase NTCDI-4, and β phase NTCDI-4 are shown in blue, green, and red, respectively. The α phase NTCDI-4 spectrum is calculated by subtracting the spectrum of the α phase NTCDI-1 template from the absorbance spectrum of the solvent-vapor annealed stack shown in panel d.

molecular orientation and morphology in organic compounds.[38] Leveraging this idea, we deposited NTCDI-4 atop α phase NTCDI-1 thin films to test whether the presence of the α phase of NTCDI-1 can help destabilize the β phase of NTCDI-4 and seed the growth of its previously inaccessible α phase. The absorbance spectra and GIXD patterns of the α phase of NTCDI-1 and β phase of NTCDI-4 are shown in Figure 5a,b for reference. When NTCDI-4 is deposited atop the α phase of NTCDI-1 (Figure 5c), its absorbance spectrum and GIXD pattern are different from that of its pure β phase. Deconvolution of the absorbance spectrum indicates the presence of both its α and β polymorphs. This coexistence is further supported by the presence of (*hkl*) reflections associated with its α phase (white arrows) and β phase (red arrows) in the GIXD pattern collected on the stack. That we can now destabilize the β phase of NTCDI-4 and access the α phase when its β phase was previously resistant to any polymorphic transformation implicates heteroepitaxial growth as a means for overcoming the kinetic barrier of this transformation. We further subjected the NTCDI-1/NTCDI-4 stack to post-deposition annealing. Solvent-vapor annealing this stack readily converts the β-phase portion of NTCDI-4 to its α phase (Figure 5d). In the same manner, thermal annealing the stack converts the α-portion of the NTCDI-4 film to its β phase, as tracked by GIXD and absorbance (Figure 5e). That the β-to-α phase transformation of NTCDI-4 occurs when α-phase domains are already present suggests that nucleation of the α-phase polymorph is the bottleneck for the transformation for which we attribute the presence of short contacts as the barrier.

CONCLUSIONS

Our results shed light on the important characteristics that allow for rapid screening of polymorphic stability in molecular materials. First, subtle changes to the molecular chemistry do not necessarily impact how these derivatives pack in the solid state. Indeed, the NTCDI compounds generally adopt the same one-dimensional π-stack packing motif when they access their α phases and the same two-dimensional brickwork-packing motif when they access their β phases. Further supporting this assertion is a report on fluorinated NTCDIs.[39] With fluorines in lieu of chlorines, the α-phase crystals of these NTCDI compounds still adopt a one-dimensional π-stack packing motif that is similar to those of the α-phase crystals of the NTCDIs studied here. Subtle changes in chemistry can, however, substantially impact the noncovalent interactions in these molecular crystals. Changes that result in interlayer short contacts between neighboring molecules in a given packing

DOI: 10.1021/jacs.8b01421
J. Am. Chem. Soc. 2018, 140, 7519−7525

motif can lock the molecules in place and stabilize the polymorph; transformation away from this packing motif becomes substantially more difficult regardless of whether it is the enthalpically favored polymorph. Our study suggests this framework to be widely applicable to molecular semiconductors, as we have highlighted with the NTCDI derivatives, TIPS and TES Pn, TMS DBC, and C6 DBTDT. This observation further extends to offset TIPS Pn and PDIF-CN2 (Figures S5–S6), each of which remains arrested in a polymorph that exhibits interlayer short contacts. A literature survey highlights many more examples of molecular semiconductors (Table S15) whose polymorphic transformations, or lack thereof, can be correlated with the absence or presence of interlayer short contacts, respectively. In the notable example of rubrene, polymorphic transformation between its triclinic and orthorhombic phases has never been reported despite the fact that these two phases have been independently accessed.[40,41] Perhaps not so coincidentally, the crystal structures of both its polymorphs exhibit short interlayer contacts. Although the orthorhombic polymorph is predicted to be thermodynamically stable at all temperatures,[42] our framework suggests the presence of interlayer short contacts to kinetically stabilize the triclinic polymorph of rubrene when it is accessed, which in turn impedes its transformation to the orthorhombic phase.

Our framework appears not limited to molecular semiconductors adopting layered structures. We have tested it on a wide range of organic compounds, ranging from pharmaceutics to biological building blocks, the details of which are tabulated in Table S15. We find that in general (for both layered and network structures), the presence of short contacts in all three dimensions locks the molecules in place while the absence of short contacts in at least one dimension provides an extra degree of freedom for molecular rearrangement, thus allowing for polymorphic transformations. Case in point is ROY, whose polymorphic stabilities are consistent with our short-contact framework. While ROY has two distinct conformers, bringing about differences in conformational polymorphs, we can compare across the polymorphs within each conformer to deconvolute the effects of conformational polymorphism on our framework. This comparison indicates the presence of short interlayer contacts in each of the polymorphs. These short contacts arrest the packing arrangements, kinetically stabilizing the different polymorphs for time frames ranging from months to years. Similarly, the β phase of anhydrous guanine exhibits interlayer short contacts that are not present in its α phase, which may be responsible for why the β phase is uniquely observed at physiological conditions. While slurry-based experiments indicate the thermodynamically favored α phase grows at the expense of the β phase, this process takes place through dissolution and recrystallization (solid–liquid–solid) as opposed to a polymorphic transformation (solid–solid).[43] In this era of machine learning and materials by design, computational advances have enabled predictions of available packing motifs given the chemical structure of a compound.[44,45] By assessing the intermolecular short contacts present in these different polymorphs, our framework can help identify which polymorphs, among them, are practically accessible and stable, ultimately extending the predictive power of the solid-state properties of the compound prior to synthesis.

■ ASSOCIATED CONTENT

Supporting Information

The Supporting Information is available free of charge on the ACS Publications website at DOI: 10.1021/jacs.8b01421.

Tables of crystaligraphic data (CIF)
Tables of crystaligraphic data (CIF)
Tables of crystaligraphic data (CIF)
Tables of crystaligraphic data (CIF)
Tables of crystaligraphic data (CIF)
Details regarding single-crystal growth, structural characterization, and experimental procedures; crystal structures; 2D-GIXD images; DFT and SAPT calculation results; and literature survey of interlayer short contacts (PDF)

■ AUTHOR INFORMATION

Corresponding Author

*lloo@princeton.edu

ORCID

Antonio Facchetti: 0000-0002-8175-7958
John E. Anthony: 0000-0002-8972-1888
R. Thomas Weitz: 0000-0001-5404-7355
Chad Risko: 0000-0001-9838-5233
Yueh-Lin Loo: 0000-0002-4284-0847

Present Addresses

○Department of Physics, CeNS, and Nanosystems Initiative Munich, Ludwig Maximilians Universität München, 80799 Munich, Germany.
^Department of Chemistry, Tianjin University & Collaborative Innovation Center of Chemical Science and Engineering, Tianjin, 300072, China.

Author Contributions

The manuscript was written through contributions of all authors. All authors have given approval to the final version of the manuscript.

Notes

The authors declare no competing financial interest.

■ ACKNOWLEDGMENTS

G.E.P. and Y.-L.L. would like to thank Dr. Leeor Kronik for useful discussions and Drs. Sean Parkin and Phil Jeffrey for crystal-structure determination. A portion of this work was conducted at the Cornell High Energy Synchrotron Source (CHESS), which is supported by the National Science Foundation (NSF) under Award DMR-1332208. G.E.P. acknowledges financial support from the Department of Defense (DoD) through the National Defense Science and Engineering Graduate Fellowship (NDSEG) Program. G.E.P. and Y.-L.L. acknowledge NSF funding under Award DMR-1627453, as well as that from the Princeton Center for Complex Materials, a MRSEC supported by NSF under Award DMR-1420541. C.R. and J.E.A. acknowledge the NSF under Award DMR-1627428, and C.R. thanks the University of Kentucky Vice President for Research for start-up funds. Supercomputing resources on the Lipscomb High Performance Computing Cluster were provided by the University of Kentucky Information Technology Department and Center for Computational Sciences (CCS).

DOI: 10.1021/jacs.8b01421
J. Am. Chem. Soc. 2018, 140, 7519–7525

REFERENCES

(1) Sutton, C.; Risko, C.; Brédas, J.-L. *Chem. Mater.* **2016**, *28* (1), 3.
(2) Cruz-Cabeza, A. J.; Reutzel-Edens, S. M.; Bernstein, J. *Chem. Soc. Rev.* **2015**, *44* (23), 8619.
(3) Bauer, J.; Spanton, S.; Henry, R.; Quick, J.; Dziki, W.; Porter, W.; Morris, J. *Pharm. Res.* **2001**, *18* (6), 859.
(4) Datta, S.; Grant, D. J. W. *Nat. Rev. Drug Discovery* **2004**, *3* (1), 42.
(5) Wille, R. L.; Lutton, E. S. *J. Am. Oil Chem. Soc.* **1966**, *43* (8), 491.
(6) Li, J.; Brill, T. B. *Propellants, Explos., Pyrotech.* **2007**, *32* (4), 326.
(7) Luzzati, V. *Curr. Opin. Struct. Biol.* **1997**, *7* (5), 661.
(8) Yang, J.; Hu, C. T.; Zhu, X.; Zhu, Q.; Ward, M. D.; Kahr, B. *Angew. Chem., Int. Ed.* **2017**, *56* (34), 10165.
(9) Chung, H.; Diao, Y. *J. Mater. Chem. C* **2016**, *13*, 773.
(10) Purdum, G. E.; Yao, N.; Woll, A.; Gessner, T.; Weitz, R. T.; Loo, Y. L. *Adv. Funct. Mater.* **2016**, *26* (14), 2357.
(11) Price, S. L.; Braun, D. E.; Reutzel-Edens, S. M. *Chem. Commun.* **2016**, *52* (52), 7065.
(12) Mandal, T.; Marson, R. L.; Larson, R. G. *Soft Matter* **2016**, *12* (39), 8246.
(13) Gavezzotti, A.; Filippini, G. *J. Am. Chem. Soc.* **1995**, *117*, 12299.
(14) Yu, L. *Acc. Chem. Res.* **2010**, *43* (9), 1257.
(15) Hirsch, A.; Gur, D.; Polishchuk, I.; Levy, D.; Pokroy, B.; Cruz-Cabeza, A. J.; Addadi, L.; Kronik, L.; Leiserowitz, L. *Chem. Mater.* **2015**, *27* (24), 8289.
(16) Guille, K.; Clegg, W. *Acta Crystallogr., Sect. C: Cryst. Struct. Commun.* **2006**, *62* (8), o515.
(17) Purser, S.; Moore, P. R.; Swallow, S.; Gouverneur, V. *Chem. Soc. Rev.* **2008**, *37* (2), 320.
(18) Hiszpanski, A. M.; Woll, A. R.; Kim, B.; Nuckolls, C.; Loo, Y.-L. *Chem. Mater.* **2017**, *29* (10), 4311.
(19) Oh, J. H.; Suraru, S.-L.; Lee, W.-Y.; Könemann, M.; Höffken, H. W.; Röger, C.; Schmidt, R.; Chung, Y.; Chen, W.-C.; Würthner, F.; Bao, Z. *Adv. Funct. Mater.* **2010**, *20* (13), 2148.
(20) He, T.; Stolte, M.; Burschka, C.; Hansen, N. H.; Musiol, T.; Kälblein, D.; Pflaum, J.; Tao, X.; Brill, J.; Würthner, F. *Nat. Commun.* **2015**, *6*, 5954.
(21) Bondi, A. *J. Phys. Chem.* **1964**, *68* (3), 441.
(22) Turner, M. J.; McKinnon, J. J.; Wolff, S. K.; Grimwood, D. J.; Spackman, P. R.; Jayatilaka, D.; Spackman, M. A. University of Western Australia, 2017.
(23) Dunitz, J. D.; Gavezzotti, A. *Acc. Chem. Res.* **1999**, *32*, 677.
(24) Dunitz, J. D. *IUCrJ* **2015**, *2*, 157.
(25) He, P.; Tu, Z.; Zhao, G.; Zhen, Y.; Geng, H.; Yi, Y.; Wang, Z.; Zhang, H.; Xu, C.; Liu, J.; Lu, X.; Fu, X.; Zhao, Q.; Zhang, X.; Ji, D.; Jiang, L.; Dong, H.; Hu, W. *Adv. Mater.* **2015**, *27* (5), 825.
(26) Jurchescu, O. D.; Meetsma, A.; Palstra, T. T. M. *Acta Crystallogr., Sect. B: Struct. Sci.* **2006**, *62* (2), 330.
(27) Forni, A.; Metrangolo, P.; Pilati, T.; Resnati, G. *Cryst. Growth Des.* **2004**, *4* (2), 291.
(28) Rowland, R. S.; Taylor, R. *J. Phys. Chem.* **1996**, *100* (18), 7384.
(29) Anthony, J. E.; Brooks, J. S.; Eaton, D. L.; Parkin, S. R. *J. Am. Chem. Soc.* **2001**, *123* (38), 9482.
(30) Chung, H.; Dudenko, D.; Zhang, F.; D'Avino, G.; Ruzié, C.; Richard, A.; Schweicher, G.; Cornil, J.; Beljonne, D.; Geerts, Y.; Diao, Y. *Nat. Commun.* **2018**, *9* (1), 278.
(31) Miyata, Y.; Yoshikawa, E.; Minari, T.; Tsukagoshi, K.; Yamaguchi, S. *J. Mater. Chem.* **2012**, *22* (16), 7715.
(32) Anthony, J. E.; Eaton, D. L.; Parkin, S. R. *Org. Lett.* **2002**, *4*, 15.
(33) Shu, Y.; Collis, G. E.; Dunn, C. J.; Kemppinen, P.; Winzenberg, K. N.; Williamson, R. M.; Bilic, A.; Singh, T. B.; Bown, M.; McNeill, C. R.; Thomsen, L. *J. Mater. Chem. C* **2013**, *1* (39), 6299.
(34) Diao, Y.; Lenn, K. M.; Lee, W.-Y.; Blood-Forsythe, M. A.; Xu, J.; Mao, Y.; Kim, Y.; Reinspach, J. A.; Park, S.; Aspuru-Guzik, A.; Xue, G.; Clancy, P.; Bao, Z.; Mannsfeld, S. C. B. *J. Am. Chem. Soc.* **2014**, *136* (49), 17046.
(35) Grieco, C.; Doucette, G. S.; Pensack, R. D.; Payne, M. M.; Rimshaw, A.; Scholes, G. D.; Anthony, J. E.; Asbury, J. B. *J. Am. Chem. Soc.* **2016**, *138* (49), 16069.
(36) Ullah Khan, H.; Li, R.; Ren, Y.; Chen, L.; Payne, M. M.; Bhansali, U. S.; Smilgies, D. M.; Anthony, J. E.; Amassian, A. *ACS Appl. Mater. Interfaces* **2013**, *5* (7), 2325.
(37) Thorley, K. J.; Finn, T. W.; Jarolimek, K.; Anthony, J. E.; Risko, C. *Chem. Mater.* **2017**, *29* (6), 2502.
(38) Campione, M.; Raimondo, L.; Moret, M.; Campiglio, P.; Fumagalli, E.; Sassella, A. *Chem. Mater.* **2009**, *21* (20), 4859.
(39) Yuan, Z.; Ma, Y.; Gessner, T.; Li, M.; Chen, L.; Eustachi, M.; Weitz, R. T.; Li, C.; Mullen, K. *Org. Lett.* **2016**, *18* (3), 456.
(40) Fielitz, T. R.; Holmes, R. J. *Cryst. Growth Des.* **2016**, *16* (8), 4720.
(41) Ndjawa, G. O. N.; Graham, K. R.; Mollinger, S.; Wu, D. M.; Hanifi, D.; Prasanna, R.; Rose, B. D.; Dey, S.; Yu, L.; Brédas, J.-L.; McGehee, M. D.; Salleo, A.; Amassian, A. *Adv. Energy Mater.* **2017**, *7* (12), 1601995.
(42) Wang, X.; Garcia, T.; Monaco, S.; Schatschneider, B.; Marom, N. *CrystEngComm* **2016**, *18* (38), 7353.
(43) Gur, D.; Pierantoni, M.; Elool Dov, N.; Hirsh, A.; Feldman, Y.; Weiner, S.; Addadi, L. *Cryst. Growth Des.* **2016**, *16*, 4975.
(44) Price, S. L. *Chem. Soc. Rev.* **2014**, *43* (7), 2098.
(45) Day, G. M. *Crystallogr. Rev.* **2011**, *17* (1), 3.

DOI: 10.1021/jacs.8b01421
J. Am. Chem. Soc. 2018, 140, 7519−7525